Dielectric Spectroscopy of Reactive Polymers

Jovan Mijovic and Benjamin D. Fitz
Department of Chemical Engineering, Chemistry and Materials Science
Polytechnic University
Six Metrotech Center, Brooklyn, NY 11201
jmijovic@poly.edu
bfitz01@utopia.poly.edu

1. Introduction

There are very good reasons for the current surge of interest in the fundamental and applied aspects of dielectric spectroscopy (DS) of polymeric materials. Fundamental investigations of the dielectric response yield a wealth of information about different molecular motions and relaxation processes. A unique characteristic of DS is the wide frequency range, from 10^{-5}Hz to 10^{11} Hz, over which polymers respond to an applied electric field. This remarkable breadth is the key feature that enables one to relate the observed dielectric response to slow (low frequency) and/or fast (high frequency) molecular events. A strong industrial interest in dielectric and electrical properties of polymers reflects the growing use of these materials in electronic interconnect devices, optoelectronic switches, printed board circuitry, microwave assemblies for radar, batteries, fuel cells, and so on.

Detailed accounts of the basic aspects of dielectric behavior of polymeric materials can be found in several books and key reviews [1-10], although the information in these sources pertains almost exclusively to the systems that do not change with time. Systematic studies by DS of systems characterized by a temporal evolution of structure have a more recent origin. The great potential of dielectric spectroscopy in such investigations has been pointed out in an excellent recent article by Williams [11]. Examples include systems that undergo a chemical and/or physical change as a result of chemical reaction, crystallization, vitrification, phase separation, etc.

In this application note we shall focus attention on the use of dielectric measurements to follow cure, i.e. the conversion of (usually) liquid prepolymers into a three-dimensional thermoset polymer network.

2. Objectives

The principal objective of this application note is to present an overview of the effect of cure on the two principal polarization mechanisms in polymers, charge migration and dipole orientation. To facilitate the understanding of the principles of dielectric cure monitoring, we shall begin in Section 3 by delineating the origins of polarization in polymers. In Section 4 we shall recap the various experimental aspects of dielectric spectroscopy. This will be followed by the description of how the advancement of cure affects charge migration (Section 5) and dipole reorientation (Section 6). Each section will summarize the fundamental background, briefly review the published information and present a few selected examples.

3. The Origin of Dielectric Response

When an electric field is applied across the faces of a parallel plate capacitor containing a dielectric, the atomic and molecular charges in the dielectric are displaced from their equilibrium positions and the material is said to be polarized. There are several different mechanism that can induce polarization in a dielectric upon the application of field. One type of induced polarization arises when electrons are displaced from their equilibrium positions with respect to the atomic nucleus and an induced dipole moment is produced. This polarization, known as electronic polarization, is extremely fast; its resonant frequency is in the ultraviolet or visible range of the electromagnetic spectrum. Another kind of induced polarization is found in molecules that consist of two different atoms, say carbon and hydrogen. The electron distribution in these molecules is not symmetrically shared, resulting in the presence of two ions with opposite charge. Application of an external field will cause deflection of these ions from their equilibrium positions, creating an induced dipole moment. This polarization is called atomic polarization, and its resonant frequency is in the infrared range of the electromagnetic spectrum. Thus both electronic and atomic polarization have high resonant frequencies that fall within the realm of vibrational spectroscopy and are considered instantaneous in dielectric spectroscopy. An important question is: which polarization mechanisms are studied by dielectric spectroscopy?

The answer is that there are two major polarization mechanisms in polymeric materials that are studied by dielectric spectroscopy: 1) polarization due to charge migration, and 2) polarization due to orientation of permanent dipoles. Let us look at charge migration first. Migration of charges gives rise to conductivity [12]. The measured conductivity encompasses contributions from extrinsic migrating charges (e.g., ionic impurities) and intrinsic migrating charges (e.g., proton transfers along hydrogen bonds). Extrinsic conductivity is commonly assumed to be inversely proportional to viscosity according to the viscous model for charge transfer (Stokes law), implying that highly viscous materials should exhibit zero conductivity, which is never the case. This means that the origin of conductivity in highly crosslinked polymer networks should be traced to the intrinsic migrating charges, whose existence in solids is documented in the literature [14-17]. Different mechanisms of intrinsic charge migration have been proposed but not systematically studied in conjunction with the ongoing chemical reactions in polymeric materials. While extrinsic conductivity decreases during reaction as a result of the increase in viscosity, intrinsic conductivity can follow a more complex pattern, and hence the trend exhibited by the overall (measured) conductivity will depend on which mechanism (extrinsic or intrinsic) dominates the dielectric response. As a direct consequence of this interplay between extrinsic and intrinsic contributions, the measured value can display different trends, as was exemplified elsewhere [18]. In Section 5 we shall describe how the progress of cure affects polarization by charge migration.

The second major polarization mechanism is dipole orientation. While electronic and atomic polarization result from *induced dipoles*, there are many materials that contain *permanent dipoles.* When such materials are placed in the electric field, dipole orientation or dipole polarization is produced as a result of the alignment of dipoles in the direction of the applied field. However, unlike the electronic and atomic polarization which are considered instantaneous by dielectric spectroscopy, the orientation (polarization) of permanent dipoles involves cooperative motions of molecular segments in a viscous medium with time-scales measurable by dielectric spectroscopy. The time-dependent loss of orientation of dipoles upon removal of the electric field is called dipole relaxation. In Section 6 we shall discuss the effect of cure on dipole dynamics.

There are two additional aspects of induced polarization that one should recognize and account for in the interpretation of experimental results. The first is electrode polarization, which results from the accumulation of ions at the polymer-electrode interface. The second aspect is the polarization due to the build-up of charges at the interface (or in the interphase) between components in heterogeneous systems. This polarization is known as interfacial, space charge or Maxwell-Wagner-Sillars.

4. Experimental

A. Principles of Measurement

Most dielectric measurements are conducted by applying voltage to the electrode interface and measuring the amplitude and the phase shift of the resulting current. The ratio of the output signal to the input perturbation is called the transfer function. If the input signal is the current and the output signal the voltage, the transfer function is the system impedance. Similarly, if the input signal is the voltage and the output signal the current, the transfer function is the system admittance, Y. Since both the amplitude and the phase angle of the output may change with respect to the input values, the impedance, Z, is expressed as the complex number; $Z = Z' - iZ''$, where Z' and Z'' are the real and imaginary components of impedance, respectively. In addition to impedance and admittance, there are several other derived quantities that can be obtained from dielectric spectroscopy. These include the dielectric modulus, the complex dielectric constant (or dielectric permittivity) and the susceptibility. The interrelations between all these parameters are tabulated elsewhere [19].

B. Instrumentation

By a broad definition, the frequency range of dielectric measurements varies from 10^{-5} Hz to 10^{11} Hz. Early descriptions of methodology and instrumentation for dielectric measurements can be found in the classic text by McCrum, Read and Williams [1] and the book by Hedvig [3], while an in-depth treatment of dielectrics at microwave frequencies can be found in the fine book by Methaxas and Meredith [20]. Most recently, an excellent review of the instrumentation for broadband dielectric spectroscopy was written by Kremer and Arndt [21]. It is fair to say that a strong existing interest in the use of dielectric spectroscopy is primarily a consequence of the recent developments in instrumentation capable of performing automatic frequency sweeps from micro-hertz to giga-hertz range. A literature survey shows that the instruments most widely used by the research community are 1) Solartron 1260 gain phase impedance analyzer, operable in the frequency range from 10^{-5} Hz to 32 MHz, and 2) Hewlett-Packard 4284A precision LCR meter, operable in the range from 20 Hz to 1 MHz. For highly accurate low-frequency measurements of samples with high impedance, an active interface must be used [22, 23]. High frequency measurements, above 1 MHz, are much less common. Among the commercial instruments that operate in that range, Hewlett-Packard 4291A RF impedance analyzer is most often mentioned. At present, Novocontrol is the leading company that offers complete setups for dielectric measurements that include instruments, high-precision heating/cooling control, various accessories, a wide range of software, and so on.

C. Cells and Sensors

In the course of a dielectric measurement voltage is applied across the sample between two conductive electrodes. The most commonly used types of electrodes are parallel plate, and comb. Acquisition and interpretation of data is readily achieved with parallel plate electrodes but the control of plate area and spacing must be extremely accurate for quantitative analysis. The reproducibility of data obtained with comb electrodes may be superior but these are typically larger than the parallel plate electrodes. In either case, a bridge is designed to calculate the impedance (or admittance) between the electrodes when the field is applied. The signal is then processed and the dielectric constant calculated from the measured values of impedance.

In the early eighties an improved technique for in-situ measurements of dielectric properties has been developed and termed microdielectrometry [24]. The microdielectrometer sensor is a comb electrode fitted with a pair of field-effect transistors that combines the best features of parallel plate and comb electrodes. When a microdielectrometer sensor is placed in the electric field, it measures the so-called complex transfer function (which is related to the admittance) from which the dielectric constant is calculated. A detailed description of this sensor is available in the literature [25]. Another sensor for in-situ monitoring of cure, known as frequency-dependent electromagnetic sensor (FDEMS) has been developed by Kranbuehl [26]. It is commercially available as DekDyne microsensor, has an area of ca. 2.5x1.2cm and is about 125microns. Further details regarding this sensor are available elsewhere [26-28]. Similar sensors for in-situ monitoring of cure at microwave frequencies are not currently available, although the concept of microwave dielectrometry has been put forward.

D. In-Situ Real Time Monitoring of Cure

One particularly attractive aspect of dielectric measurements is their applicability to in-situ real time monitoring of chemical and physical processes. The concept of in-situ dielectric monitoring of processing holds great appeal for materials and process engineers, with the principal advantages being three-fold. First,

the in-situ acquired information eliminates the need for off-line collection and analysis of control samples. Second, dielectric measurements have a distinct advantage over other characterization techniques of being able to monitor cure continuously, as the resin changes from viscous liquid to gel to highly crosslinked glass. And third, the fundamental character of the sensed information allows a continuous verification of chemo-physical changes inside the reactor against a known processing model and provides an input for "smart" closed-loop process control. The key characteristic of a smart or intelligent system is its ability to self-adjust to the variations in the material and/or processing parameters and thus guide the process along an optimum path.

Over the years, thermocouples and pressure transducers were almost exclusively used for in-situ monitoring of cure. Precise monitoring of temperature is particularly important in thick composites, where high reaction exotherms and low heat dissipation rates could result in considerable temperature gradients within the sample, but the knowledge of temperature as a function of time and location offers little insight into the molecular nature of cure. The pressure gradient across the thickness of the composite is important in the analysis of resin flow but alone, like temperature, reveals little about what happens on the molecular level. Dielectric measurements have the advantage of providing a more fundamental response that could be related to the two main processing parameters, namely degree of cure and viscosity. Naturally, the use of dielectric measurements is not limited to the in-situ monitoring of processing of polymers and composites. Attractive possibilities for their use exist in diverse fields, including the microelectronic industry, the pharmaceutical industry for measurements of dissolution rates of tablets and capsules, the chemical industry for polymerization, separation, extraction and catalytic processes, and so on.

5. Polarization due to Migrating Charges

A. Modeling Concepts - Equivalent Circuits

One of the most attractive features of dielectric spectroscopy lies in its applicability to the studies aimed at the development of direct correlations between the response of a real system and an idealized model circuit composed of discrete electrical components. In the modeling studies one seeks to match experimental impedance with the impedance of an equivalent circuit composed of ideal resistors and capacitors. General accounts of models based upon equivalent circuitry have been given in several key references [19, 29-31], but their use in the studies of polymers has a much more recent origin.

Phenomenologically, a resistance (R) is taken to represent the dissipative component of the dielectric response, while a capacitance (C) describes the storage component of the dielectric, i.e. its ability to store the electric field. Resistance(s) and capacitance(s) can be combined in a variety of forms, leading to an array of phenomenological models that can describe various combinations of polarization mechanisms in dielectric materials. Inductance (L) requires the storage of energy in a magnetic field, but there is no appreciable AC magnetic field energy present in the low current (mA) DS measurements.

The simplest equivalent circuits are obtained by combining resistance and capacitance in parallel or series. An R-C parallel circuit (Figure 1A), its simplicity notwithstanding, is often an adequate model of polarization by charge migration in a given frequency range. A single resistance that encompasses the dissipative contributions of all migrating charges, extrinsic and intrinsic alike, is all that is needed to describe the overall loss because the dissipative contributions due to electrode polarization and dipole relaxations occur at lower and higher frequencies respectively. The lone capacitance, on the other hand, embodies the overall ability of the dielectric to store the electric field by all polarization mechanisms. The overall impedance of a parallel circuit, (equal to the reciprocal overall admittance, Y), is given by the sum of the contributions from resistance and capacitance:

$$\vec{Z} = \frac{1}{\vec{Y}} = \frac{1}{\frac{1}{R_1} + i\omega C_1} \qquad (1)$$

where i is $(-1)^{1/2}$ and ω is the angular frequency, $\omega=2\pi f$. The real and imaginary components of impedance are given by:

$$Z' = \frac{R_1}{1 + (\omega C_1 R_1)^2} \qquad (2)$$

and

$$Z'' = -i\frac{\omega C_1 R_1^{\,2}}{1 + (\omega C_1 R_1)^2} \qquad (3)$$

where RC is equal to τ, the circuit characteristic time. In the case of dipole polarization, τ is called the relaxation time. Two (or more) charge-migration mechanisms that are well-separated in the frequency domain can be modeled by a series of two (or more) R-C parallel circuits.

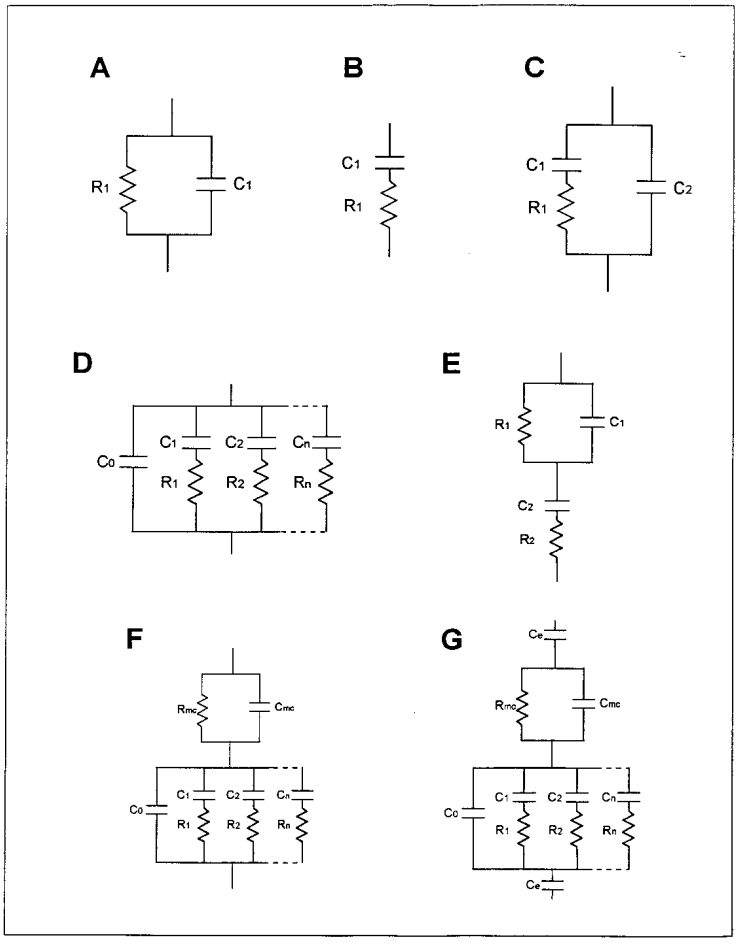

Fig. 1 : Circuit diagrams for the modeling of material properties.

When resistance and capacitance are placed in series (Figure 1B), the resulting combination leads to the classic Debye equations for a single dipole or many dipoles with a single relaxation time. In reality, however, the contribution to the stored energy from atomic and electronic polarization is always reflected in the measured dielectric response, and that is accounted for in the models by introducing an additional capacitance (C^1) in parallel with the dipole contribution (C^2-R series). The overall admittance of that circuit (Figure 1C) is given as:

$$\vec{Y} = i\omega C_2 + \frac{i\omega C_1(1 - i\omega\tau)}{1 + (\omega\tau)^2} \qquad (4)$$

where $\tau = R_1C_1$. This expression is often reported in terms of the complex dielectric constant $\varepsilon^* = Y/(i\omega\varepsilon_0)$

$$\varepsilon^* = \varepsilon'_\infty + \frac{(\varepsilon'_0 - \varepsilon'_\infty)}{1 + i\omega\tau} \qquad (5)$$

By separating equation 5 into its real and imaginary components we obtain:

$$\varepsilon'(\omega) = \varepsilon'_{\infty} + \frac{\left(\varepsilon'_0 - \varepsilon'_{\infty}\right)}{1 + (\omega\tau)^2} \quad (6)$$

$$\varepsilon''(\omega) = -i\frac{\left(\varepsilon'_0 - \varepsilon'_{\infty}\right)\omega\tau}{1 + (\omega\tau)^2} \quad (7)$$

Equations 6 and 7 are commonly referred to as Debye equations. When plotted in the complex plane (ε'' versus ε'), equations 6 and 7 yield a semicircle of radius $(\varepsilon_0-\varepsilon_\infty)/2$ known as the Cole-Cole plot [32].

Inherent in equations 6 and 7 is the assumption of a single relaxation time. In polymeric materials, however, the mobility of different dipoles depends upon the local restrictions imposed by their immediate surroundings. The spatial variation of these restrictions results in a distribution of relaxation times. An equivalent circuit that accounts for the distribution of relaxation times is shown in Figure 1D. Analytically, a distribution of relaxation times can be taken into account in different ways, as described in Section 6.

Let us now consider several equivalent circuits characterized by the presence of two or more polarization mechanisms. For example, the elements of circuit 1E represent the following dielectric events: capacitance C^{mc} includes the contributions of atomic and electronic polarization, as well as the capacitance (i.e. non-lossy contribution, *if any*) inherent in polarization by migrating charges; resistance R^{mc} represents the dissipative component of polarization due to migrating charges; capacitance C^2 and resistance R^2 describe dipole(s) with a single relaxation time. An equivalent circuit that, in addition to the above phenomena, also accounts for a distribution of relaxation times, can be modeled as shown in Figure 1F. Finally, particularly at low frequencies it is often important to take into account the presence of electrode-blocking layers, which introduce an infinite resistance to the passage of current and can be modeled with two additional capacitances (C^e) in series, shown as identical in Figure 1G.

B. Graphical Representation and Evaluation of Characteristic Parameters

We shall now briefly describe the various methods of graphical representation of impedance data and the quantitative evaluation of circuit parameters of an R-C parallel circuit. The first representation is based on the plots of imaginary versus real impedance, often referred to as Nyquist plots. An example of a Nyquist plot for the formulation composed of a difunctional epoxy resin (diglycidylether of bisphenol-A, or DGEBA) and diethylenetriamine (DETA) curing agent, following the cure at 50°C for 10 minutes, is given in Figure 2A. An R-C parallel equivalent circuit yields a semicircle in the complex plane, with the resistance obtained form the intersection of the semicircle and the Z' axis. The second representation of impedance data consists in plotting the absolute value of impedance, $|Z| = [(Z')^2 + (Z'')^2]^{1/2}$, as a function of the logarithm of frequency. The resulting Bode plot has the characteristic shape shown in Figure 2B.The value of resistance is obtained from the intersection of the extrapolated frequency-independent horizontal line and the log|Z| axis. At higher frequency the dielectric response is purely capacitative and impedance is directly proportional to frequency with a slope of -1. The third graphical representation is based on the plots of imaginary impedance as a function of frequency. An example of such plot is shown in Figure 2C. In general, three zones characterize this type of plot: a low frequency zone where electrode polarization dominates, an intermediate frequency zone where polarization by migrating charges plays a major role, and a high frequency zone where dipole relaxation takes place. Figure 2C shows the intermediate zone, up to 1MHz in this case, where the dielectric response is not affected by either electrode polarization or dipole relaxation. In many real situations, the dielectric response in a given frequency range reduces to a simple R-C parallel model whose imaginary impedance is given by equation 3. Taking the derivative of Z'' with respect to angular frequency, we get:

$$\frac{dZ''}{d\omega} = \frac{CR^2\left(1 - \left(\omega\,\mathrm{RC}\right)^2\right)}{1 + (\omega CR)^2} \quad (8)$$

Equation 8 is equal to zero at the peak in the Z'' versus frequency plot and that condition is met for ω=1/RC. By combining equations 3 and 8 we obtain:

$$Z''^{max} = R/2 \quad (9)$$

which enables one to calculate the unknown resistance directly from the plot ($R=2*Z''^{max}$).

Naturally, the numerical values of the elements of model circuits change in the course of chemical reaction. The progress of reaction is followed by performing frequency sweeps over as broad as possible frequency interval. It is important to assure that the time-scale of the experiment is negligible in comparison with the time-scale of the structural changes in the system, so that each measurement can be taken to represent an isostructural state. As an illustration of the changes in Z" vs. frequency as the material cures, we present Figure 3, where changes in both the $Z"_{max}$ peak location and peak intensity can be observed.

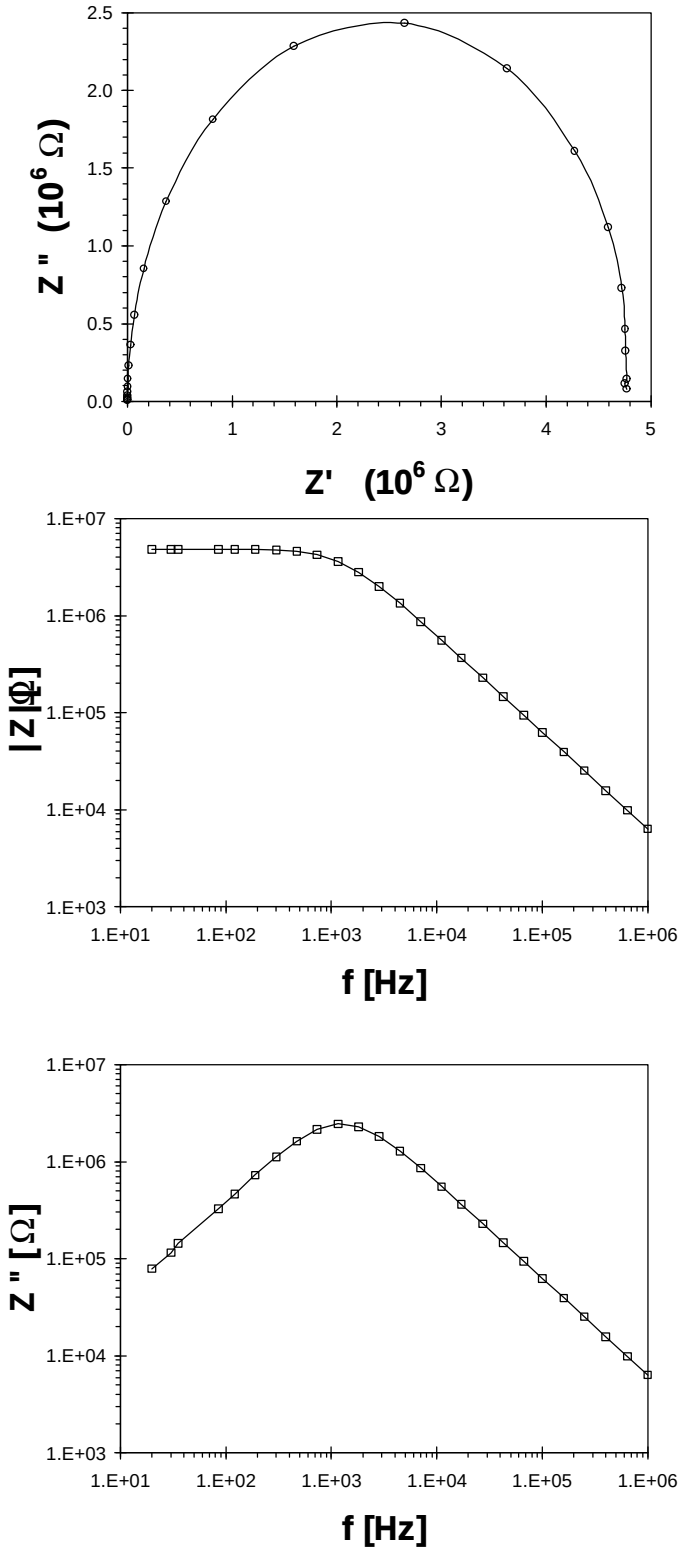

Fig. 2 : ***A***. Imaginary part of complex impedance vs. real part of impedance for a crosslinking system after 10 minutes of cure. ***B***. Modulus of impedance vs. frequency for the system in plot A. ***C***. Imaginary part of complex impedance vs. frequency for the system in plot A.

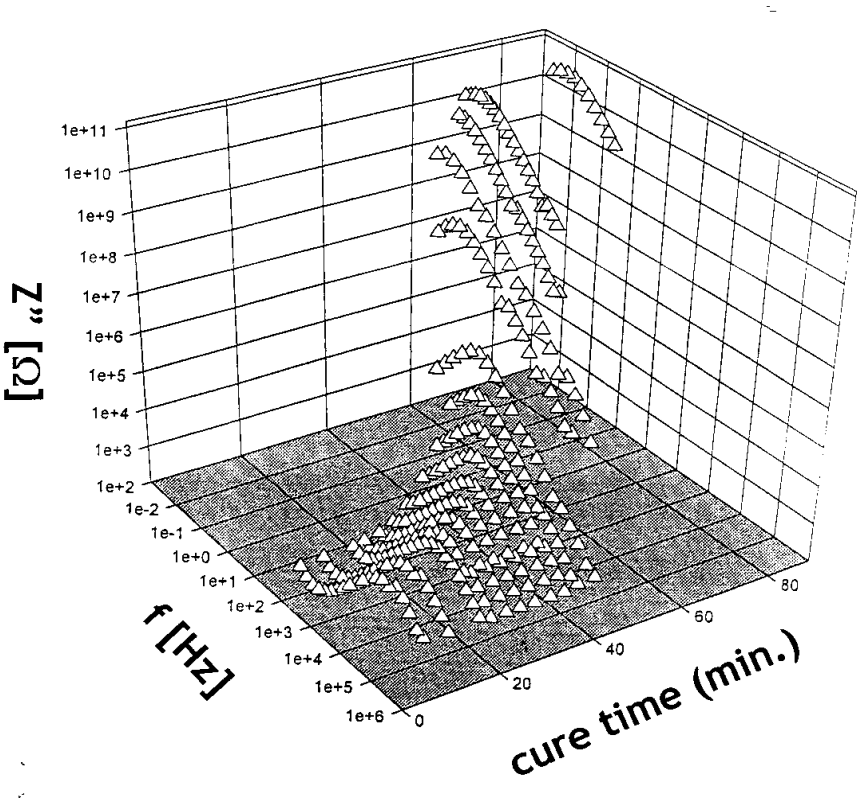

Fig. 3 : 3-D plot of imaginary part of impedance vs. frequency as a function of cure time for the reactive system presented in figure 2.

Reverting to the above described methodology and utilizing spectra of the type shown in Figure 2C obtained at various stages of cure, we calculate resistance from equation 9 as a function of reaction time. Next, the resistivity, ρ (or its reciprocal - conductivity, σ=1/ρ) is calculated from the following equation:

$$\rho = RS/L \qquad (10)$$

where S/L is the cell constant. Figure 4 is an example of the changes in conductivity vs. cure time for an isothermal reaction at several temperatures of a trifunctional epoxy triglycidylether of paraaminophenol (TGEPA) and a tetrafunctional amine methylenedianiline (MDA) formulation.

The extent of reaction (or degree of cure), α, is then obtained from resistivity using an empirical equation which most often takes the following form:

$$\frac{\alpha}{\alpha_m} = \frac{\log(\rho) - \log(\rho_0)}{\log(\rho_m) - \log(\rho_0)} \qquad (11)$$

Here, α_m denotes the maximum value of extent of reaction attainable at a given cure conditions prior to vitrification [33], ρ_m is the corresponding resistivity, while the subscript 0 denotes the initial conditions. An example, Figure 5, illustrates a comparison of cure kinetics obtained via this technique for the reactive system in Figure 4 vs. those obtained with infra-red spectroscopy - the agreement is quite good.

Finally, equation 11 (or another empirical equation) could be substituted into a chemorheological expression that enables one to calculate viscosity during cure. An example is equation 12 proposed by Kenny et al. [34]:

$$\eta = \eta_{g0} \exp\left[\frac{C_{1\eta}\left[T - T_g(\alpha)\right]}{C_{2\eta} + T - T_g(\alpha)}\right]\left[\frac{\alpha_g}{\alpha_g - \alpha}\right]^n \qquad (12)$$

where η_{go}, C_{1n}, C_{2n}, and n are parameters to be obtained by a fitting procedure and α_g is the extent of cure at gelation. It was successfully utilized in their study of the cure of a tetraglicidyl diaminodiphenyl methane (TGDDM) epoxy and diphenyl diaminosulfone (DDS) amine. A good agreement between the measured viscosity and the prediction of phenomenological models based on dielectric data was reported for both isothermal and non-isothermal cure. An example comparison of the model predictions to experimental data is shown in Figure 6 for a constant heating rate of 3°C/min.

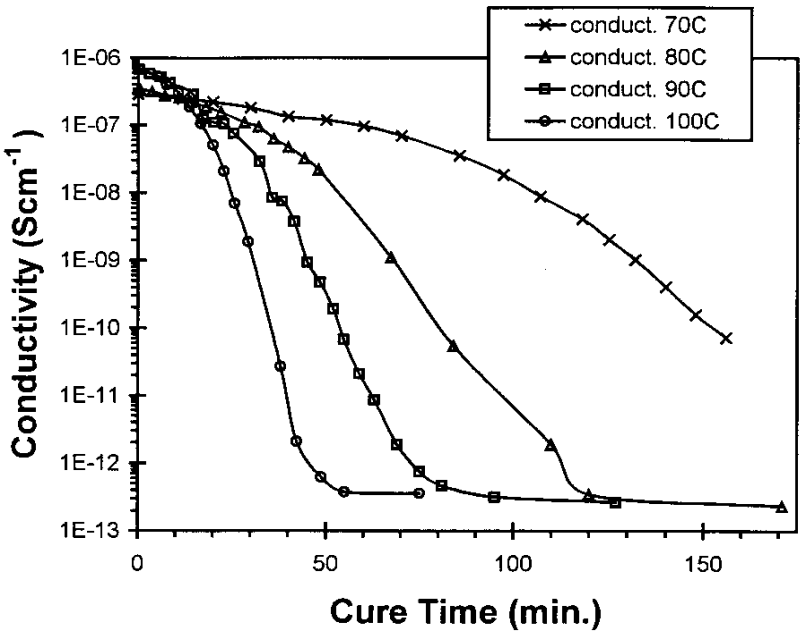

Fig. 4 : Conductivity vs. cure time at several isothermal reaction temperatures for an epoxy/amine reactive system (see text for material details).

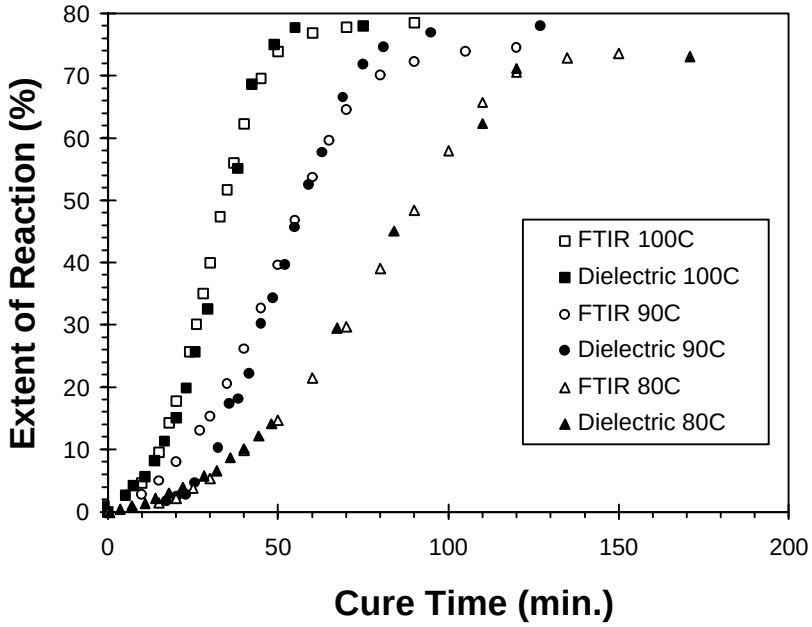

Fig. 5 : Comparison of extent of reaction calculated via equation 11 from *in-situ* dielectric spectroscopy to those obtained via *in-situ* Fourier-transform infra-red spectroscopy.

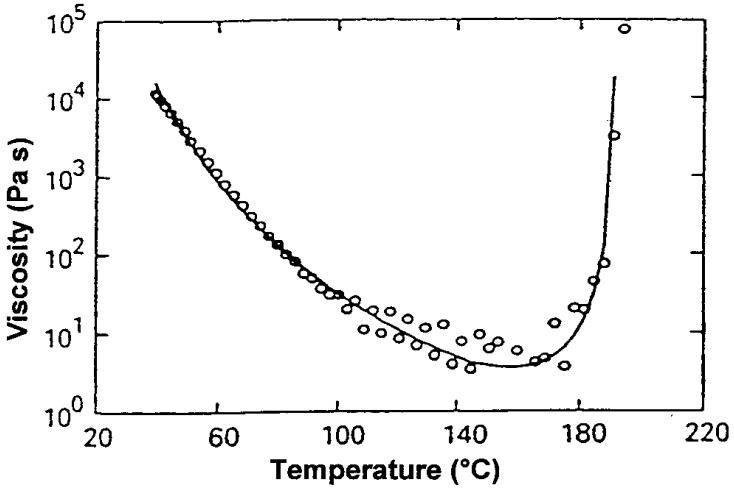

Fig. 6 : Dynamic viscosity vs. temperature monitoring and model predictions (eqn. 12, solid line) for a curing system (see text for material details).

C. Examples of In-Situ Dielectric Cure Monitoring

We begin this section by emphasizing that an early review of the dielectric analysis of thermoset cure was written by Senturia and Sheppard in the mid-eighties [35] and several reviews have appeared subsequently [36, 37]. Most recently, Kranbuehl [38] wrote an excellent article on the dielectric monitoring of polymerization and cure, in which he showed a number of examples of the use of sensors to monitor the dielectric response during cure in molds, autoclaves, adhesives, films and coatings. Consequently, our goal here is not to be comprehensive but rather to highlight the most interesting aspects of this subject and present a few representative examples.

Following the introduction of dielectric sensors in the eighties, a number of investigators [39-44] and particularly Kranbuehl and coworkers [45- 47] have continued to use sensors for in-situ monitoring of processing. The emphasis in those studies, however, was predominately on the application of sensors and instruments to a growing number of different materials while the essential features of their analyses have remained unchanged.

The starting point in the analysis of dielectric data is the following equation:

$$\varepsilon'' = \frac{(\varepsilon_0 - \varepsilon_\infty)\omega\tau}{1+(\omega\tau)^2} + \frac{\sigma}{\omega\varepsilon_0} \qquad (13)$$

The main premise in this approach is that at some experimental frequency the contribution of dipole loss to the total loss is negligible and hence:

$$\frac{(\varepsilon_0 - \varepsilon_\infty)\omega\tau}{1+(\omega\tau)^2} << \frac{\sigma}{\omega\varepsilon_0} \qquad (14)$$

With this inequality equation 13 becomes:

$$\varepsilon'' = \frac{\sigma}{\omega\varepsilon_0} \qquad (15)$$

The apparent conductivity, which is of interest and is commonly referred to in the literature as “ionic conductivity”, can then be calculated from:

$$\sigma = \omega\varepsilon_0\varepsilon'' \qquad (16)$$

This apparent conductivity has been identified as the dielectric parameter of interest because it can be related, at least qualitatively, with the fundamental processing parameters such as degree of cure and viscosity.

In the crucial processing stage of thermoset networks before gelation, ionic conductivity is inversely proportional to viscosity, while the time derivative of ionic conductivity mimics the rate of cure. Also, the temperature dependence of ionic conductivity can be modeled by the classic WLF equation. In practice, the inequality expressed by equation 14 is met at some frequency which is not known a priori. Two methods for the calculation of ionic conductivity of thermoset polymers based on this approach have been described by Day and coworkers [e.g. 25] and Kranbuehl and coworkers [26-28]. Fundamentally, the two methods differ little and were contrasted from the point of view of accuracy and reproducibility in the fine paper by Ciriscioli and Springer [48].

An example of in-situ dielectric monitoring of impregnation and cure during processing of a composite structure is described below [49]. In Figure 7 we show a graphite preform of a "T" support, with the location of dielectric sensors indicated by numbers 1 through 9. The preform is in a mold in an autoclave. A vacuum is maintained and a tetra-functional epoxy/amine formulation is introduced at the bottom. Figure 8 shows changes in temperature and conductivity during cure at locations 1 (Fig. 8A) and 3 (Fig. 8B). As the temperature rises the resin impregnates the fiber preform, reaching sensor 1 at 45 minutes and sensor 3 at 170 minutes. The $\varepsilon''\omega$ lines monitor ionic conductivity, which tracks the changes in resin viscosity, first rising with temperature and then dropping as the resin cures.

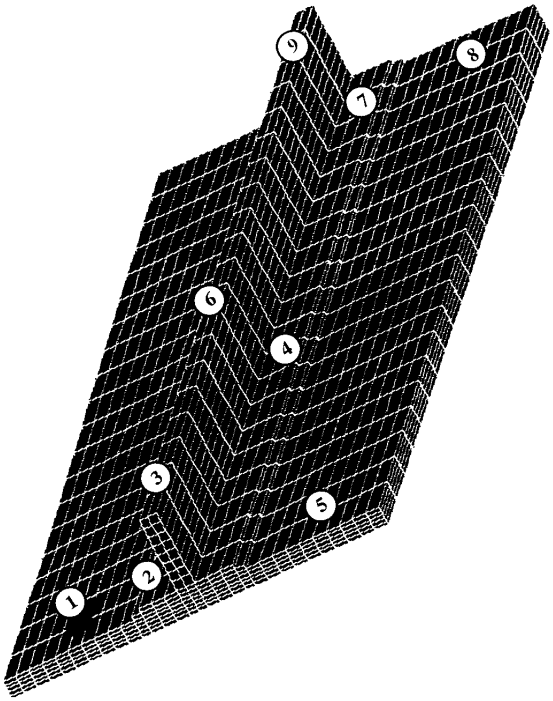

Fig. 7 : Diagram of "T" support. The location of dielectric sensors is indicated by numbers 1 through 9.

At this point it is appropriate to comment briefly on the usefulness and limitations of the use of ionic conductivity for in-situ monitoring of cure. It is our opinion that the following three principal requirements must be met before a complete and successful implementation of this methodology is possible:
1) the availability of sensors and instruments for fast, reliable and reproducible measurements of the dielectric response during cure;
2) the development of a fundamental understanding of the basis of measured conductivity, and;
3) the development of models that relate the measured dielectric response to the chemorheological characteristic of the resin.

What is the current status? The first requirement has been largely met. The second and third requirement have not. Ionic conductivity is calculated assuming that some ions are initially present in the resin formulation. Although that is probably true, neither the type and concentration of such ions nor their effect on the measured response have been identified, much less systematically studied. When one considers a large variety of resin formulations and the inevitable vicissitudes of the batch-to-batch characteristics and their hygro-thermal

histories, it is clear that any model based on the measured conductivity is bound to be empirical and batch-specific. Further research along these lines is warranted. Nonetheless, it is also true that, notwithstanding the lack of fundamental a fundamental picture of the measured phenomena, dielectric spectroscopy is the only currently available technique for in-situ monitoring of kinetics and rheology of cure.

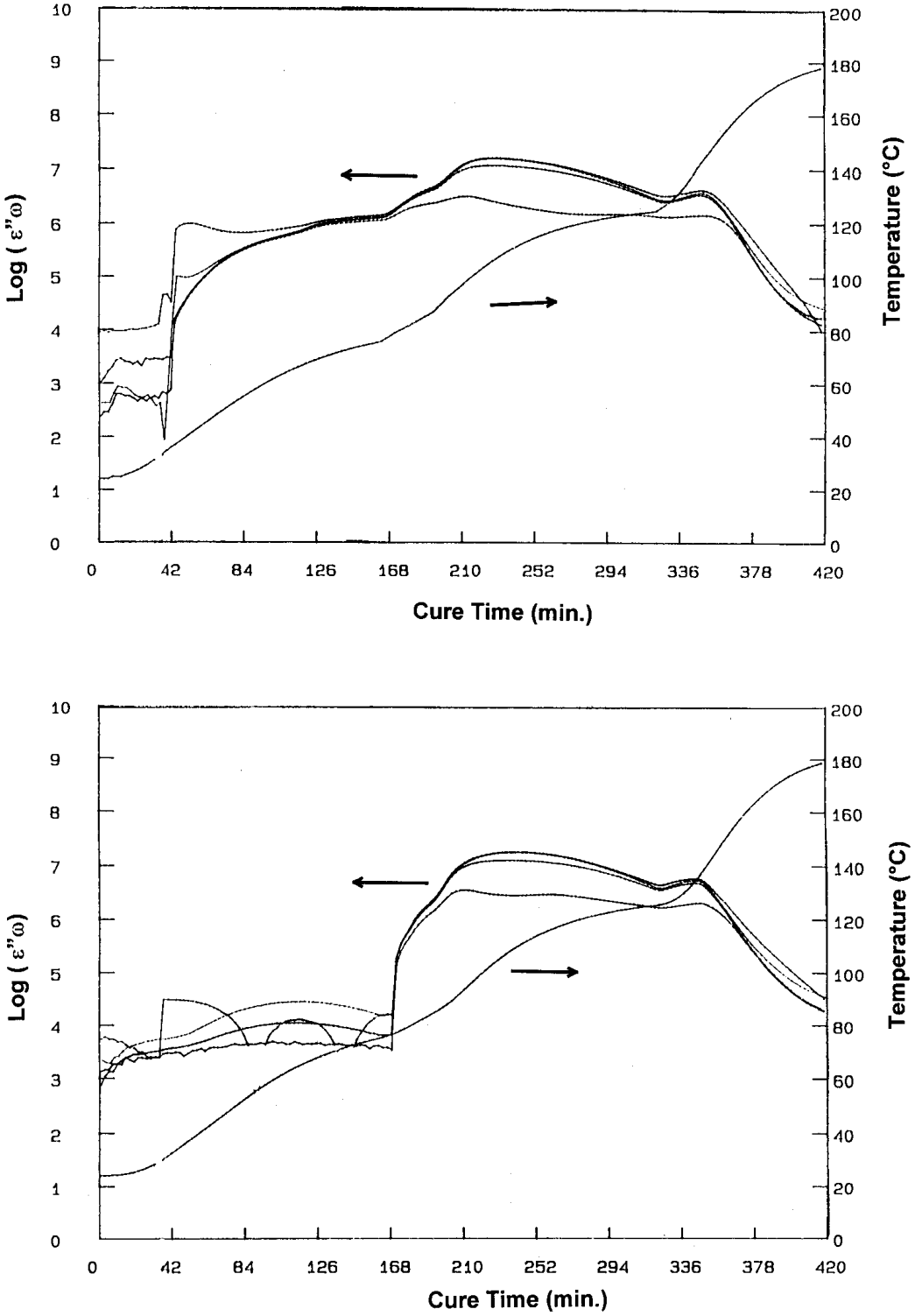

Fig. 8 : Changes in temperature and conductivity with cure time as monitored at locations 1 (upper plot ***A***) and 3 (lower plot ***B***) in "T" support of Fig. 7.

6. Polarization by Dipole Orientation

An advantage of wide band DS is its ability to probe molecular dynamics (of dipoles) at all times during cure: from the early stages of a high temperature cure, where the dipolar relaxation times are on the order of tens of picoseconds (~10GHz) to the late stages of cure (after gelation) through the vitrification process where the glassy state relaxation times are tens to hundreds of seconds. Throughout cure, accompanying the relaxation time changes, are changes in: static dielectric constant, high frequency dielectric constant (index of refraction), the shape parameters of the relaxation peak, and the separation of secondary, high frequency local relaxation processes. We will discuss these changes in turn and show examples of how cure may be monitored by experimental observation of them.

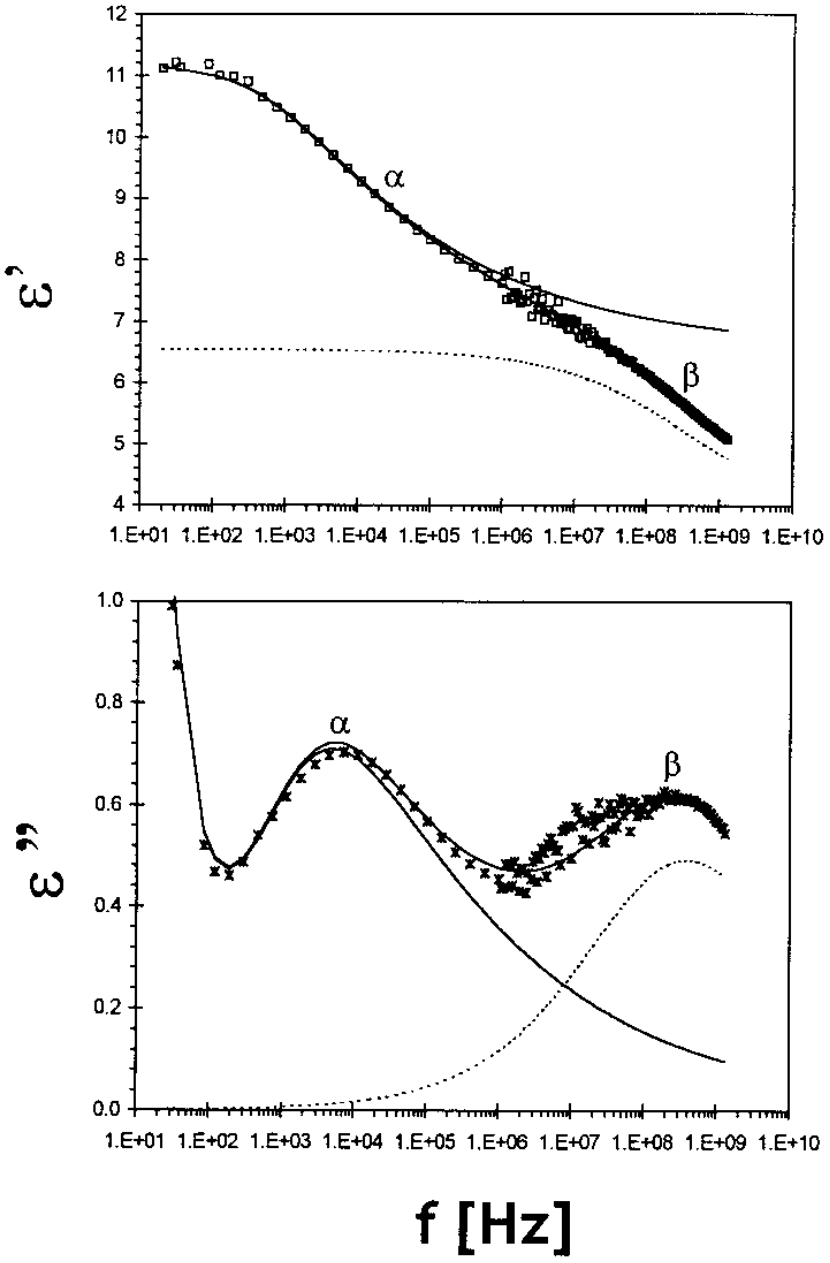

Fig. 9 : Dielectric constant and loss vs. frequency for DGEBA/DETA reactive system at 45% cure, 50°C, α and β processes indicated. Dark solid curve through data is HN function (equation 21), lighter and dashed curves are deconvoluted α and β processes.

A. Dipolar Relaxation Processes: α, β

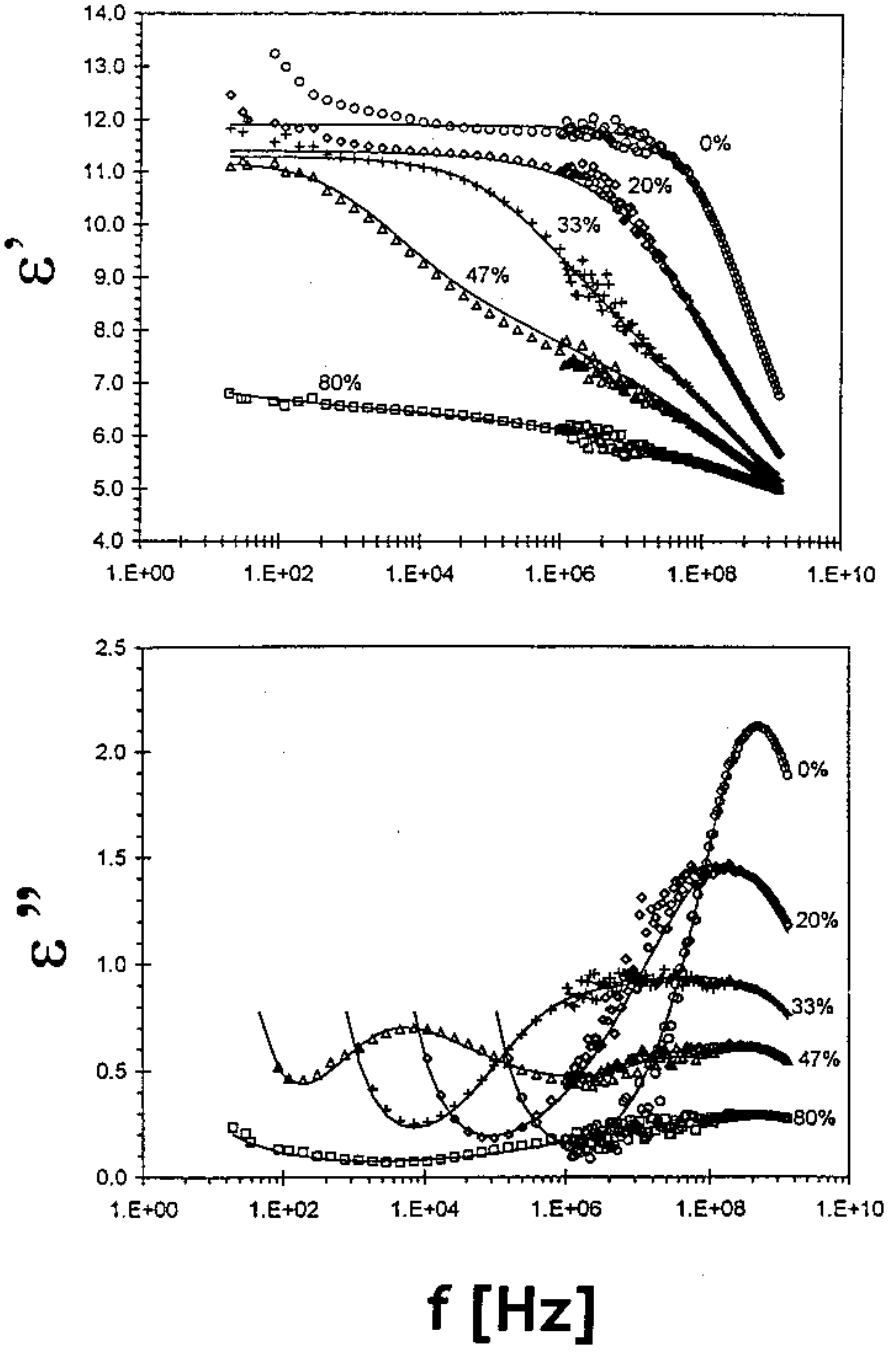

Fig. 10 : Dielectric constant and loss vs. frequency for DGEBA/DETA reactive system at indicated degrees of cure for isothermal chemical reaction at 50°C.

Distinct from charge migration polarization at low frequencies and the very high frequency ($f \sim 10^{14}$Hz) atomic and electronic polarizations lies the polarization due to the motion of permanent dipoles in a material. The type of resulting dipolar motion to an applied electric field perturbation will depend on the length-scale of motion. At high frequencies there are often found secondary relaxation peaks which are broad, have Arrhenius temperature dependence, low activation energy ~5kcal/mol-K, low intensity, and are also present below Tg. The origin of these so-called β relaxations remains elusive, but appeals have been made in the literature to explanations ranging from far-IR phonon excitations [50], cage-rattling motions [51], a universal glassy-state

phenomena [52], and various types of local/side-chain motions [1]. For the purpose of this article we rest with only the naming of the process. The larger primary relaxation process is associated with the glass transition. It consists of cooperative segmental motions and generally exhibits a non-Arrhenius, but strong, temperature dependence. It is conventionally named the α process. At high temperatures (and therefore frequencies) the α and β processes merge; the faster-moving (w/ temperature) α process catches up with and merges with the slower β process to become the αβ process. To illustrate clearly a typical permittivity spectrum for an amorphous epoxy resin at a temperature above Tg we present Figure 9. Plotted are both dielectric constant and loss frequency dependence with the α and β processes labeled. The illustration will serve as a point of reference in the following discussion of permittivity spectral changes with cure.

B. Changes In Relaxation Time (τ)With Cure

In order to effectively and accurately monitor and later analyze a time dependent change in a material, such as crystallization, phase separation, or chemical reaction, a measurement must be of a fundamental material property, independent of the specific type of test. While other types of measurement may be sensitive to the material change, a fundamental analysis will not be possible. The dipolar relaxation time, a fundamental material parameter, will be shown to be an effective tool for the study of reactive systems.

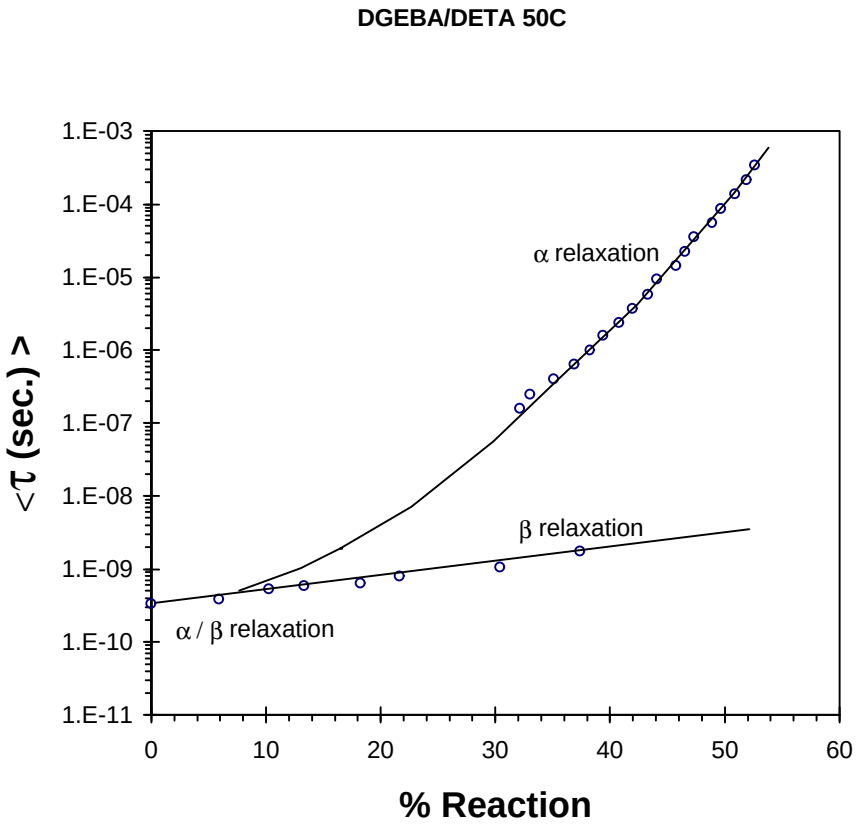

Fig. 11 : Apparent relaxation time vs. degree of cure for reactive system of Fig. 10.

For a typical epoxy/amine formulation undergoing isothermal cure, we present in Figure 10 dielectric constant and loss in the frequency domain with extent of cure as a parameter. During cure, as molecular weight and connectivity increase and the accompanying bulk physical properties develop (Tg rises, mechanical properties are enhanced) the dipolar dynamics encounter the three regimes illustrated in Figure 10. They are: regime I—early cure, merged, αβ process, picosecond relaxation time; regime II—the α and β processes separate with the α at lower frequencies; and regime III—near the completion of cure, at which time the α process shifts to very low frequencies (indicating glass formation), while the secondary β process remains at high frequencies. To more clearly indicate the divergence of the αβ process we extract from Fig. 10 the relaxation times, τ, $\tau=1/(2\pi*fmax)$, where fmax is the frequency of the ε" peak, and plot in Figure 11 log τ as a

function of conversion for all of the above regimes. The curve running through the data is a modified version of the WLF/VF functional form [53] for the α process:

$$\tau_\alpha = \tau_{0\alpha} \exp\left(\frac{F_1}{\% - \%(0)}\right) \quad (17)$$

and for the β process, a simple exponential, Arrhenius-like equation:

$$\tau_\beta = \tau_{0\beta} \exp\left(F_2 * \%\right) \quad (18)$$

where % is degree of cure, and $\tau_{0\alpha}$, $\tau_{0\beta}$ F_1 and F_2 are best-fit parameters to the data in Figure 11. The change in τ originates from both an increase in the materials viscosity and its Tg. We point out that τ, for α and β processes, does not diverge to infinity at the gel-point as translational processes do, since the segmental, α–type processes become independent of molecular weight above a material-dependant critical chain-length.

A strategy for the monitoring of cure via τ dynamics can now be briefly outlined (additional details may be found in the recent literature [54, 55]). The first step is to perform a series of measurements on the material at selected isothermal reaction temperatures. These runs will serve as calibration reference runs. Curing reactions may then be performed under any thermal/reaction time history within the temperature bounds of the reference runs. Initially, the degree of cure (via DSC, FTIR, titration, GPC etc.) vs. reaction time at various temperatures as well as the accompanying dipolar τ changes are needed. Then by applying a general kinetic rate equation:

$$\frac{d\alpha}{dt} = k * f'(\alpha) f''(\alpha) \quad (19)$$

where k is a temperature dependent rate constant and $f'(\alpha)$ and $f''(\alpha)$ are factors to account for kinetic considerations such as an autocatalytic mechanism or a diffusion controlled reaction step. Utilizing the temperature dependent rate constants, an activation energy is obtained which allows the determination of sample composition and degree of cure under any thermal history (within the temperature limits of the original data). Next the relaxation time data are analyzed. An assumption can be made on the form of τ dynamics with reaction: log τ=logτ0-k*τ/ln(10) as experimentally observed over the typical frequency /reaction time windows. The activation energy for the k and τ0 temperature dependencies are calculated, resulting in an expression for τ for any (limited) thermal history. Combining the chemical kinetic model and the τ model we have a model for τ as a function of extent of reaction. Ultimately, any applied thermal history (within the temperature range of the original kinetic calibration) can be used together with the measured τ to arrive at extent of cure. The foregoing methodology is applicable to a feed-back smart-sensor style of processing technology.

C. Relaxation Strength

A second approach to cure monitoring based on dipole polarization is the characterization of the extremes in dielectric constant: static ε'_0 and high frequency ε'_∞ or the difference— $(\varepsilon'_0 - \varepsilon'_\infty) = \Delta\varepsilon'$, relaxation strength. The motivation behind this approach is, as we shall see, a direct relationship between a materials dipole composition and the static permittivity, ε'_0. Since, in general, during cure the dipolar composition changes in a systematic manner, measurement of ε'_0 will give fundamental information on the makeup of the reactive system at any time during cure. We will explore the relations between relaxation strength and the materials constitutive dipoles after a brief introduction.

The primary requirement for monitoring a chemical reaction using dipolar relaxation spectroscopy is, of course, that there be present some polar portion of one of the reactants and/or products. That requirement being met, there are four chemical reaction possibilities: 1. the dipoles present in the reactants are not involved in the chemical reaction so that the product contains the same concentration (normalized for density changes) and type of dipolar groups (e.g., telechelic polymer chains with reactive end-groups—such as vinyl-terminated siloxane polymers) ; 2. the reactant dipoles are involved in the reaction and a new type of dipole is formed (e.g., a reactive mixture of epoxide and amine containing molecules); 3. the reactant dipoles form non-polar groups (e.g., cyanate ester resins which crosslink to form symmetric non-polar triazine rings); 4. a situation where no dipoles are present among the reactants, but are formed during the chemical reaction (e.g.,

oxidation of polyethylene from radiation crosslinking). Historically the usual types of chemical reactions monitored by DRS are those in which the reactants are low molecular weight liquids and on exposure to appropriate conditions (usually heating or exposure to radiation (UV or microwave) or the addition of a catalyst) react to form various polymeric structures: linear and branched polymers [56] and crosslinked networks [26, 35, 36, 38, 54, 55, 57-60], with various physical states: viscous liquids, rubbery gels, or amorphous or semi-crystalline solids. This diversity being governed by the functionality of the reactants and the thermodynamic and kinetic chemical considerations.

Accompanying the chemical change and increase of molecular weight is usually a density increase and therefore an increase in the dipole density that should result in an increase in dipolar relaxation strength. However, an increase in permittivity is usually not observed for reactive systems because in most instances product dipoles are less polar or non polar entities. An exception has recently been found [55] where the product dipoles are of a higher dipole moment than the reactants via a possible specific interaction induced molecular conformation.

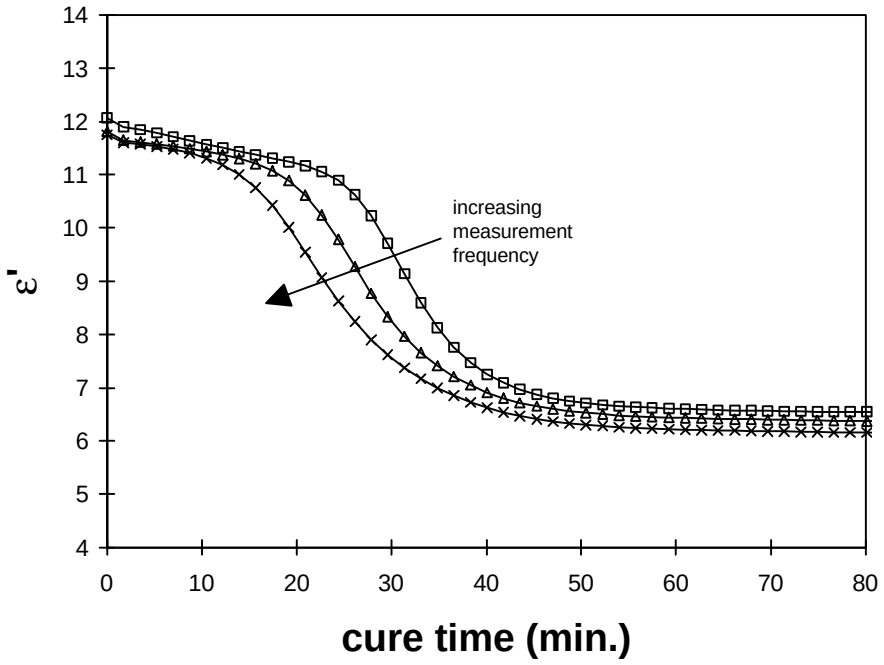

Fig. 12 : Dielectric constant vs. cure time for isothermal cure at 100°C (material details in text).

The relation between relaxation strength and a materials constituent dipoles has been derived from fundamental principals by Debye, later modified by Onsager and Fröhlich [61] as

$$\frac{\left(\varepsilon_0' - \varepsilon'_\infty\right)\left(2\varepsilon'_0 + \varepsilon'_\infty\right)}{\varepsilon'_0\left(\varepsilon'_\infty + 2\right)^2} = \frac{4\pi}{9kT}\sum N_i \left\langle \mu_i^2 \right\rangle \qquad (20)$$

where ε'_0 and ε'_∞ are the limiting low and high frequency dielectric constant, N_i is the concentration of dipoles of type i in the material, μ_i the type *i* dipole moments, k the Boltzman constant, and T the absolute temperature. In situations where the reactant dipole moments are greater than the products, which is the case for most epoxy-amine systems, a systematic decrease in ε'_0 or $\Delta\varepsilon'$ will be found. This trend is shown in Figure 12 where three measurement frequencies are used. In the early stages of cure the decrease in ε' is gradual, later when the system vitrifies an abrupt drop results. In the early reaction stages (pre-vitrification) what is being measured are changes in the materials ε'_0. However, in the reaction time window of vitrification, we are instead measuring a continuous change from ε'_0 to ε'_∞ (the materials lowest permittivity value, ignoring for the moment any β relaxations, as they have for the present purpose negligible relaxation strengths [62]). As the foregoing isochronal approach is a typical (prevailing) one in the literature, it will be useful to explore these ideas further using a series of illustrations. We show in Figure 13 A a set of frequency sweeps which

represent qualitatively the general trend for dielectric constant changes during cure. While in Figure 13 B we extract isochronal information as a function of cure time. We point out the ε'_0 changes can only be monitored while the majority of the relaxation process remains in the available experimental frequency window. That condition fails eventually because the lowest measured frequency must be kept sufficiently high so that the measurement time is short compared with chemical changes. It is this vitrification time period in cure where modeling approaches are needed to account for the dependence of the α relaxation on Tg—including the relaxation strength, relaxation time, and shape parameters. We discuss these features in a following section.

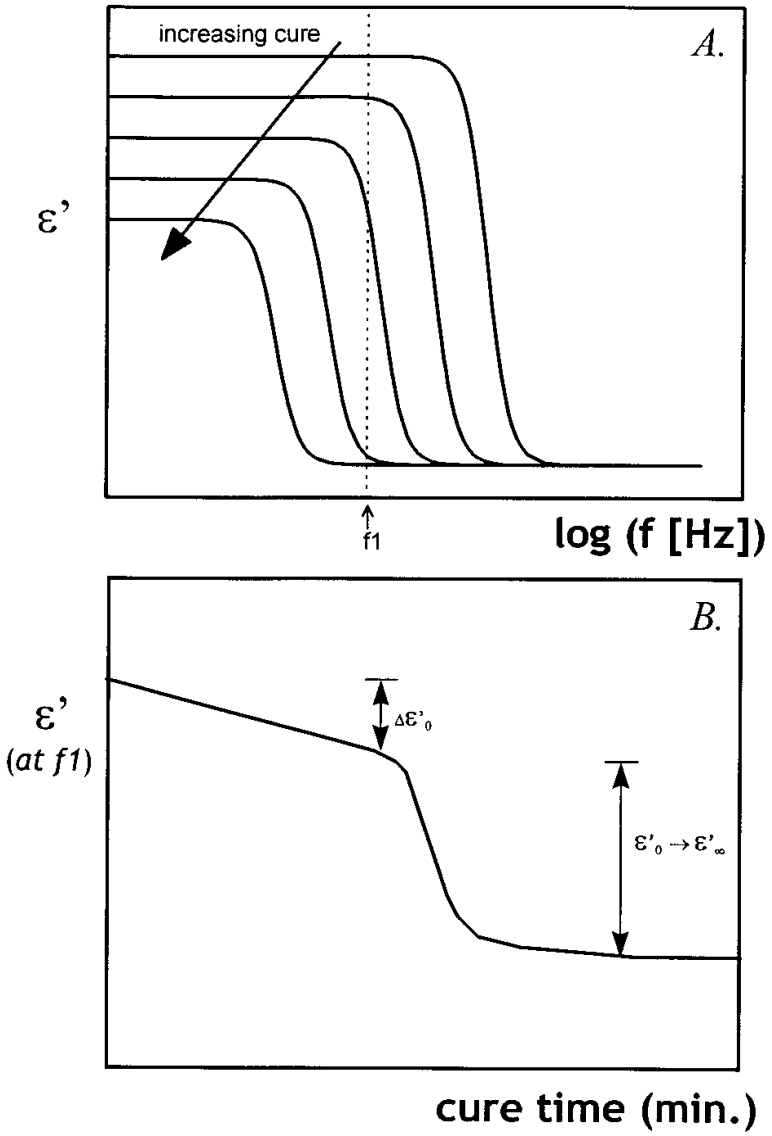

Fig. 13 : ***A***. Illustration of dielectric constant vs. frequency with cure time as a parameter.
B. Extracted dielectric constant at frequency (f1) vs. cure time for material in ***A***.

It should be mentioned that care must be exercised when presenting isochronal data to avoid choosing a frequency which includes interfacial or electrode blocking influences, as discussed in the previous section on polarization by migrating charges.

In an industrial application, microwave frequency measurements are often useful for both cure monitoring and for material characterization (particularly necessary when processing materials with microwave heating). As mentioned in the charge migration polarization section, typically at frequencies greater than 1MHz the only relevant polarization mechanisms are the dipolar relaxation and faster resonance processes. For this reason electrode effects and conductivity contributions to the measurement are avoided.

Great strides have been made in high frequency instrumentation and signal analysis techniques [63, 64] which result in rapid and accurate microwave band frequency measurements on reactive systems where disposable sensors are necessary. For industrial processing purposes it may be sufficient to monitor a dielectric response at a single microwave frequency if the material permittivity changes during cure are systematic. The types of probes used are either flat surface strip-line measurements [65], coaxial airlines filled with sample [66-68], open-ended semi-rigid coaxial lines terminated by a volume of the sample [69], or resonant cavities tuned to a specific frequency band and adjusted to obtain the samples permittivity [70, 71]. While such isochronal measurements reveal little about the underlying molecular nature of the relaxation process, and are batch-specific empirical processing methods, for industrial cure monitoring they can be useful.

D. Shape Parameters

A third approach the analysis of cure data is to examine changes in the shape parameters of a fit relaxation function. The most robust and general function is the well-known Havriliak-Negami (HN) [72]:

$$\varepsilon^*(\omega) = \frac{\varepsilon_0 - \varepsilon_1}{\left[1+\left(i\omega\tau_\alpha\right)^{1-a\alpha}\right]^{a\alpha}} + \frac{\varepsilon_1 - \varepsilon_\infty}{\left[1+\left(i\omega\tau_\beta\right)^{1-\alpha\beta}\right]^{b\beta}} + \varepsilon'_\infty - i\left(\frac{\sigma}{\omega\varepsilon_{spa.}}\right)^d \qquad (21)$$

where both the α and β processes are accounted for (see appropriate subscripts) and ω is the angular frequency, i is $(-1)^{1/2}$, ε'_0- ε'_1 and ε'_1-ε'_∞ are the relaxation strengths of the α and β processes, τ_α and τ_β are their relaxation times, a_α, b_α and a_β ,b_β are the processes shape parameters. The final term in equation 21 accounts for conductivity (σ), ε_{spa} is the permittivity of free space and d is a scaling constant, usually with a value of one for migrating charge polarization. In Figure 9 we have applied this functional form to the data. It is apparent that one of the strengths of this analysis is the ability to deconvolute distinct, but overlapped processes. We hasten to add that as the nature of the β process is poorly understood, so to the nature of the merging region of α and β. The case has not been firmly established for the independence of α and β processes [73], therefore the linear deconvolution may eventually be found to be in error. However, trends in the behavior of the relaxation times beyond this region where the processes appear to be distinct are reasonable; until these issues are resolved its continued use for this purpose is still warranted.

Other functional forms such as the Kohlrausch-Williams-Watts (KWW) [74] stretched-exponential functional form are also often applied

$$\phi(t) = A\exp\left[-\left(\frac{t}{\tau}\right)^\beta\right] \qquad (22)$$

where τ is the relaxation time and β is the stretching exponent ranging from zero to one.
This form has also been applied to isochronal cure data [75], where a modified version of the normalized complex permittivity ($\omega\tau_0$ is substitued for ω) is used:

$$\varepsilon^*\left(\omega\tau_0\right) = \varepsilon'_\infty + \left(\varepsilon'_0 - \varepsilon'_\infty\right)\int_0^\infty \exp(-i\omega\tau)\left(-\frac{\partial\phi}{\partial t}\right)dt \quad , \qquad (23)$$

$$\phi(t) = \exp\left(-\frac{t}{\tau_0}\right)^\gamma \qquad (24)$$

where ϕ is the polarization decay function, τ_0 is the modified KWW function relaxation time and the other variables have their previously defined meanings. In this isochronal method of data fitting the γ parameter represents an average of the KWW β parameter that would be found from a frequency sweep over the experimental time range of the isochronal ε" peak. It is a less precise shape parameter determination than the frequency domain method, however it may be necessary to undertake under constrained experimental situations, and can still be somewhat revealing.

There are several different fundamental physical arguments for the description of the α process [76-78] which arrive at a functional form for the relaxation phenomena in the form of a stretched-exponential (KWW). Perhaps one of the most accessible arguments is the work of Ngai [79] in which systematic changes to polymer structures were observed to result in systematically altered α process Tg-reduced temperature dependencies.

The trends as predicted from the fundamental argument become visually convincing when presented in the "cooperativity plot" (or "fragility plot" [80]) in which log τ is presented as a function of Tg/T. For our purposes we extract from that work the relation between enhanced cooperativity (stronger temperature dependence in the T->Tg limit, and broader relaxation) with a lower KWW β parameter. Additional details regarding cooperativity dynamics in a curing system may be found in the recent literature [23].

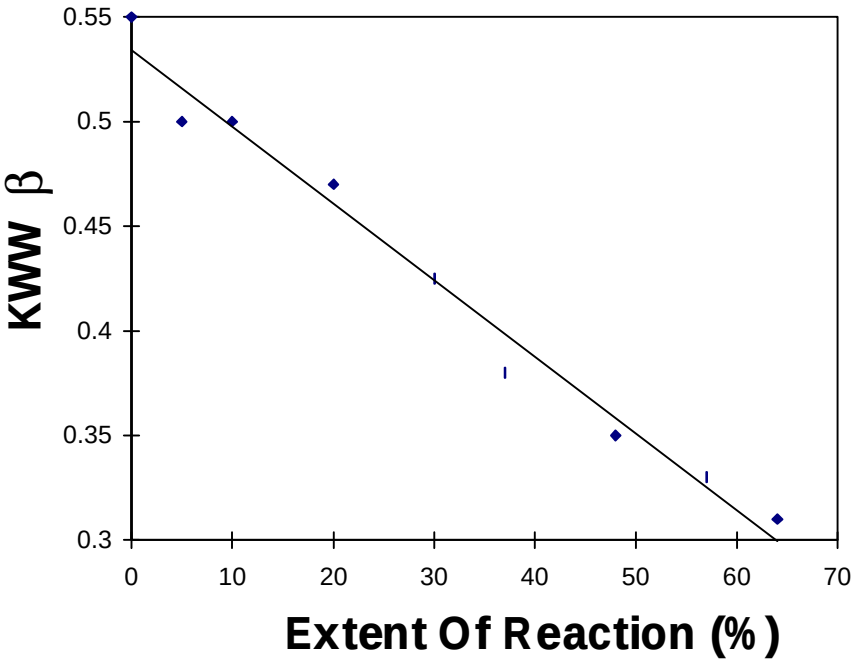

Fig. 14 KWW β parameter changes with degree of cure.

We mention finally the two power law form of Jonsher [6]:

$$\varepsilon'' \propto \omega^{m} \quad , \quad \omega << \omega_0 \qquad (25)$$

$$\varepsilon'' \propto \omega^{-n} \quad , \quad \omega >> \omega_0 \qquad (26)$$

where $\omega_0=1/\tau$. It has been explored recently in the context of curing systems[81, 82], in an attempt to ascribe significance to the slopes (m and -n) on either side of the relaxation peak in terms of length scales of motion being probed—low frequency side applying to long length-scales and the high frequency side to short; the short time n parameter arrived at by a percolation model for the glass transition [83] was found to be in agreement with their experimental findings. Historically, the interpretation of shape parameters in terms of the length-scale of the relaxation originated with the work of Schonhals and Scholsser [84] on non-reactive amorphous polymer systems.

In general, after the splitting of the $\alpha\beta$ peak early in cure, the α peak tends to broaden as crosslinkig develops. Let us examine the changes in model parameters with cure using the familiar epoxy/amine reactive system. The HN parameters (eqn. 21) show the following trends: the 1-aα linearly decreases, the bα is insensitive to cure the 1-aβ and bβ both increase and then decrease in a parabolic trend with minima occurring at the same cure time. Interpretation of these complex trends is avoided by the other models with fewer parameters. Nevertheless, the patterns in HN relaxation time changes with cure accurately reflect the apparent relaxation times gleaned from the frequency sweep data and therein lies the utility of the model. The trend in the Jonsher model m and n parameters are a constant linear decrease in m with cure from 1 to 0.5 up to 65% of conversion, while n also shows a linear decrease but with a more gradual slope from 0.4 to 0.2. In this way the systematic broadening of the α process is quantified. Finally, the KWW β parameter reveals the same broadening trend, while containing only one parameter. KWW β decreases from 0.5 to 0.32 up to 65% conversion. We show in Figure 14, the changes in KWW β parameter with cure. For this system the linear

changes in the shape parameter allow for the direct monitoring of conversion to just beyond the gel-point. The limitation to the highest extent of cure which can be covered by a relaxation peak shape analysis, comes from an experimental concern: the low frequency measurement time can not exceed appropriate values determined by the system's chemical kinetics. Perhaps in the near future a technique will be developed with a greatly reduced low frequency measurement time.

The use of changes in a model parameter to monitor cure is not appropriate for all types of reactive systems. In some reactive systems the changes are too small to be accurately monitored. A reactive urethane system, for example, exhibits a very small change in the Jonscher m and n parameters: m from approximately 0.85 to 0.8, while n changes from 0.2 to 0.25 [85]. In this system the product of the reaction is a lightly crosslinked rubber, where the final Tg of the system is much lower than the reaction temperature, and the relaxation time of the α process remains in the MHz region at completion of cure. In this case the broadening of the α process due to cooperativity on approaching the glass transition does not play a role.

7. References and Notes

1. McCrum, N. G.; Read, B.; Williams, G. Anelastic and Dielectric Effects in Polymeric Solids, Wiley, NY 1967.
2. Karasz, F. E. Ed., Dielectric Properties of Polymers, Plenum Press, NY 1972.
3. Hevig, P. Dielectric Spectroscopy of Polymers, Adam Hilger, Bristol 1977.
4. Bottcher, C. J. F.; Bordewijk, P. Theory of Electric Polarization, Elsevier, Amsterdam 1978.
5. Williams, G. Adv. Polym. Sci. 1979, 33, 60.
6. Jonscher, A. K. Dielectric Relaxation in Solids, Chelsea Dielectric Press, London 1983.
7. Ku, C. C.; Liepins, R. Electrical Properties of Polymers, Hanser, Munich 1987
8. Owen, J. in Comprehensive Polymer Science, Allen, G.; Bevington, J. C. Eds., Pergamon Press, Oxford 1988, Vol. 2, pp. 669-686.
9. Williams, G. in Comprehensive Polymer Science, Allen, G.; Bevington, J. C. Eds., Pergamon Press, Oxford 1988, Vol. 2, pp. 601-632.
10. Riande, E.; Saiz, E. Dipole Moments and Birefringence of Polymers, Prentice Hall, NY 1992.
11. Williams, G. in Keynote Lectures in Selected Topics of Polymer Science, Riande, E. Ed., CSIC, Madrid 1997, Chapter 1, pp. 1-40.
12. Conductive polymers, where charge carriers are electrons and electron holes, will not be discussed here and the reader is referred to the excellent article by Block [13].
13. Block, H. Adv. Polym. Sci. 1979, 33, 93.
14. Bockris, J. O'M.; Reddy, A. K. N. Modern Electrochemistry, Vol. 1 and 2, Plenum Press, NY 1970.
15. Barker, R. E. Jr. Pure Appl. Chem. 1976, 46, 157.
16. Seanor, D. A. Ed. Electrical Properties of Polymers, Academic Press, NY 1982.
17. Gray, F. M. Solid Polymer Electrolytes, VCH Publ. NY 1991.
18. Gallone, G.; Levita, G.; Mijovic, J.; Andjelic, S.; Rolla, P. Polymer 1998, 39, 2095.
19. Macdonald, J. R. Impedance Spectroscopy, Wiley, NY 1987.
20. Metaxas, A. C.; Meredith, R. J. Industrial Microwave Heating, Peregrinus Ltd. London 1983.
21. Kremer, F.; Arndt, M. in Dielectric Spectroscopy of Polymeric Materials, Runt, J. P.; Fitzgerald, J. J. Eds., Amer. Chem. Soc. Washington, DC 1997, Chapter 2, p. 67.
22. Kremer, F.; Boese, D.; Meier, G.; Fischer, E. W. Progr. Colloid & Polym. Sci. 1989, 80, 129.
23. Fitz, B.; Andjelic, S.; Mijovic, J. Macromolecules, 1997, 30, 5227.
24. Sheppard, N. F.; Garverick, S. L.; Day, D. R.; Senturia, S. D. SAMPE Int. Symp. 1981, 26, 65.
25. Day, D. R.; Lewis, T. J.; Lee, H. L.; Senturia, S. D. J. Adhesion 1985, 18, 73.
26. Kranbuehl, D. E.; Delos, S. E.; Jue, P, K. Polymer, 1986, 27, 11.
27. Kranbuehl, D. E.; Delos, S. E.; Hoff, M.; Weller, L.; Haverty, L.; Seeley, J. SAMPE Int. Symp. 1987, 32, 338.
28. Kranbuehl, D. E.; Hoff, M.; Haverty, L.; Loos, A.; Freeman, T. SAMPE Int. Symp. 1988, 33, 1276.
29. Sluyters-Rehbach, M.; Sluyters, J. H. in Electroanalytical Chemistry, Bard, A. J. Ed. Marcel Dekker, NY 1977, Vol. 4, pp. 1-127.
30. Archer, W. I.; Armstrong, R. D. Electrochemistry, 1980, 7, 157.
31. Walter, G. W. Corrosion Sci. 1986, 26, 681.
32. Cole, R. H.; Cole, K. S. J. Chem. Phys. 1941, 9, 341.
33. Kenny, J. M.; Trivisano, A. Polym. Eng. Sci. 1991, 31, 19.

34. Opalicki, M.; Kenny, J. M. Makromol. Chem. Makromol. Symp. 1993, 68, 41.
35. Senturia, S. D.; Sheppard, N. F. Adv. Polym. Sci. 1986, 80, 1.
36. Mijovic, J.; Kenny, J. M.; Maffezzoli, A.; Trivisano, A.; Bellucci, F.; Nicolais, L. Comp. Sci. Tech. 1993, 49, 277.
37. Mijovic, J.; Bellucci, F. The Trends in Polym. Sci. 1996, 4, 74.
38. Kranbuehl, D. E. in Dielectric Spectroscopy of Polymeric Materials, Runt, J. P.; Fitzgerald, J. J. Eds., Amer. Chem. Soc. Washington, DC 1997, Chapter 11, p. 303.
39. Sanjana, Z. N. Polym. Eng. Sci. 1986, 26, 373.
40. Zukas, W. X.; Wentworth, S. E. Polym. Composites 1987, 8, 232.
41. Day, D. R.; Sheppard, D, D. Mater. Res. Soc. Symp. Proc. 1989, 142, 227.
42. Day, D. R. Polym. Eng. Sci. 1989, 29, 334.
43. Day, D. R.; Sheppard, D, D. Polym. Composites 1991, 12, 87.
44.Mathieu, C.; Boiteux, G.; Seytre, G.; Villain, R.; Dublineau, P. J. Non-Cryst. Solids 1994, 172-4, 1012.
45.Kranbuehl, D. E.; Eichinger, D.; Hamilton, T.; Clark, R. Polym. Eng. Sci. 1991, 31, 5.
46. Kranbuehl, D. E. J. Non-Cryst. Solids 1991, 131-3, 930.
47. Kranbuehl, D. E.; Kingsley, P.; Hart, S.; Hasko, G.; Dexter, B.; Loos, A. Polym. Composites 1994, 15, 297.
48. Ciriscioli, P. R.; Springer, G. S. SAMPE J. 1989, 25, 35.
49. Kranbuehl, D. private communication.
50. Angell, C. A.; Boehm, L.; Oguni, M.; Smith, D. L. J. Mol. Liq. 1993, 56, 275.
51. Johari, G. P. in Relaxations In Complex Systems, Ngai, K.; Wright, G. B. Eds., National Technological Service, 1985.
52. Johari, G. P.; Goldstein, M. J. Chem. Phys. 1970, 53, 2372.
53. Alperstein, D.; Narkis, M. Polym. Eng. Sci. 1995, 35, 284.
54. Fournier, J.; Williams, G.; Duch, C.; Aldridge, G. A. Macromolecules 1996, 29, 7097.
55. Andjelic, S.; Mijovic, J. Macromolecules, in press.
56. Carlini, L.; Livi, A.; Rolla, P. A.; Fioretto, D. J. Non-Cryst. Solids 1994, 172-174, 569.
57. Mangion, M.; Johari, G. P. J. Polym. Sci, Part B: Polym. Phys. 1990, 28, 71.
58. Maistros, G.; Block, H.; Bucknall, C.; Partridge, I. Polymer 1992, 33, 4470.
59. Bidstrup, S. A.; Sheppard, N. F.; Senturia, S. D. Polym. Eng. Sci. 1989, 29, 325.
60. Nass, K.; Seferis, J. C. Polym. Eng. Sci. 1989, 29, 315.
61. Frohlich, H. Theory of Dielectrics, Oxford Univ. Press, London 1949.
62. A careful inspection of Fig. 12 reveals at long cure time a small difference in ε' for different frequencies—this is due to the β process.
63. Wei, Y.; Sridhar, S. Rev. Sci. Instr. 1989, 60, 3041.
64. Stuchly, M.; Stuchly, S. IEEE Trans. on Instr. Meas. 1980, IM29, 176.
65. Das, N.K.; Voda, S. M.; Pozar, D. M. IEEE Trans. Microwave Theory and Techniques, 1987, MTT35, 636.
66. Cole, R. H.; Mashimo, S.; Windsor IV, P. J. Phys. Chem. 1980, 84, 786.
67. Fioretto, D.; Livi, A.; Rolla, G.; Socino, G.; Vardini, J. Phys. Condensed Matter 1994, 6, 5294.
68. Mijovic, J.; Fitz, B. Polymers For Advanced Technologies, in press.
69. Baker, K. R.; Graybeal, J. D., in Symp. on Polym. Radiation Chem., American Chem. Soc. 1991, 470.
70. Marand, E.; Baker, K.; Graybeal, J. Macromolecules, 1992, 25, 2243.
71. Jow, J.; Hawley, M.; Finzel, M.; Kern, T. Polym. Eng. Sci. 1988, 28, 1450.
72. Havriliak, S.; Negami, S. J. Polym. Sci. 1966, C14, 99.
73. Arbe, A.; Richter, D.; Colmenero, J.; Farago, B. Phys. Rev. E. 1996, 54, 3853.
74. Williams, G.; Watts, D. Trans. Farad. Soc. 1970, 66, 80.
75. Mangion, M. B.; Johari, G. P. J. Polym. Sci, Part B: Polym. Physics 1990, 28, 1621.
76. Bendler, J. T.; Shlesinger, M. F. J. Mol. Liq. 1987, 36,37.
77. Ngai, K. L.; Rendell, R. W. J. Non-Cryst. Solids 1991, 131-133, 233.
78. Chamberlin, R. V.; Kingsbury, D. W. J. Non-Cryst. Solids 1994, 172-174, 318.
79. Ngai, K. L.; Roland, M. Macromolecules 1992, 24, 5315.
80. Recently reviewed: Angell, C. A. Science, 1995, 267, 1924.
81. Casalini, R.; Livi, A.; Rolla, P. A. Phys. Rev. B 1996, 53, 564.
82. Andjelic, S.; Mijovic, J. Macromolecules 1998, 31, 2872.
83. Langier, J. M.; Luck, J. M. J. Phys. A 1987, 20, L885.
84. Schonhals, A.; Schlosser, E. Colloid Polym. Sci. 1989, 267, 125.

85. Tabellout, M.; Randrianantoandro, H.; Emery, J. R.; Durand, D.; Hayward, D.; Pethrick, R. A. Polymer 1995, 36, 4547.

For more information on Novocontrol Dielectric measurement systems, applicaitions or service, please call your local Novocontrol sales office.

Factory and Head Office

Germany: NOVOCONTROL GmbH
Obererbacher Straße 9
D-56414 Hundsangen / GERMANY

Phone: ++(0) 64 35 - 96 23-0
Fax: ++(0) 64 35 - 96 23-33
email novo@novocontrol.com
WWW http://www.novocontrol.com

Editor Application Notes
Dr. Gerhard Schaumburg

Abstracts and papers are always welcome.
Please send your script to the editor.

Agents

Benelux countries: NOVOCONTROL Benelux B.V. Postbus 231 NL-5500 AE Veldhoven / NETHERLANDS Phone ++(0) 40 - 2894407 Fax ++(0) 40 - 2859209	**Italy:** FKV s.r.l. Via Fatebenefratelli, 3 I-24010 Sorisole (Bg) Phone ++(0) 572 725 Fax ++(0) 570 507, 573 939 **contact**: Mr. Vanni Visinoni
Great Britain: NOVOCONTROL International PO Box 63 Worcester WR2 6YQ / GB Phone ++(0) 1905 - 64 00 44 Fax ++(0) 1905 - 64 00 44 **contact**: Mr. Jed Marson	**France:** Fondis Electronic Services Techniques et Commerciaux Quartier de l'Europe, 4 rue Galilée F-78280 Guyancourt Phone: ++(0) 1-34521030 Fax ++(0) 1-30573325 **contact**: Mr. Jean-Pierre Ellerbach
USA/Canada: NOVOCONTROL America Inc. 611 November Lane / Autumn Woods Willow Springs, North Carolina 27592 / USA Phone: ++(0) 919 639 9323 Fax: ++(0) 919 639 7523 **contact**: Mr. Joachim Vinson, PhD	**Korea:** HADA Corporation P.O. Box 266 Seocho, Seoul / KOREA Phone ++(0) 2-577-1962 Fax: ++(0) 2-577-1963 **contact**: Mr. Young Hong
Japan: Morimura Bros. Inc. 2 nd chemical division Morimura Bldg. 3-1, Toranomon 1-chome Minato-Ku Tokyo 105 / Japan Phone ++(0) 3-3502-6440 Fax: ++(0) 3-3502-6437 **contact:** Mr. Nakamura	**Thailand:** Techno Asset Co. Ltd. 39/16 Mu 12 Bangwa Khet Phasi Charoen Bangkok 10160 Phone ++(0) 8022080-2 Fax ++(0) 4547387 **contact**: Mr. Jirawanitcharoen